Journal of Applied Physics

Analysis of the Urbach tail in cesium lead halide perovskites

Cite as: J. Appl. Phys. **131**, 010902 (2022); https://doi.org/10.1063/5.0076712
Submitted: 27 October 2021 • Accepted: 10 December 2021 • Published Online: 03 January 2022

Naomi Falsini, Giammarco Roini, Andrea Ristori, et al.

Journal of Applied Physics PERSPECTIVE scitation.org/journal/jap

Analysis of the Urbach tail in cesium lead halide perovskites

Cite as: J. Appl. Phys. **131**, 010902 (2022); doi: 10.1063/5.0076712
Submitted: 27 October 2021 · Accepted: 10 December 2021 ·
Published Online: 3 January 2022

Naomi Falsini,[1,2] Giammarco Roini,[3] Andrea Ristori,[4] Nicola Calisi,[5] Francesco Biccari,[1,4] and Anna Vinattieri[1,4,6,a)]

AFFILIATIONS

[1]Department of Physics and Astronomy, University of Florence, via G. Sansone 1, 50019 Sesto F.no, Italy
[2]ENEA, Italian National Agency for New Technologies, Energy and Sustainable Economic Development, Fusion and Technology for Nuclear Safety and Security Department, Nuclear Safety, Security and Sustainability Division, via Martiri di Monte Sole 4, 40129 Bologna, Italy
[3]Department of Information Engineering, University of Brescia, via Branze 38, 25123 Brescia, Italy
[4]LENS, via N. Carrara 1, 50019 Sesto F.no, Italy
[5]Department of Industrial Engineering, University of Florence, via S. Marta 3, 50139 Florence, Italy
[6]INFN-Firenze, via G. Sansone 1, 50019 Sesto F.no, Italy

Note: This paper is part of the Special Topic on Defects in Semiconductors.
a)Author to whom correspondence should be addressed: anna.vinattieri@unifi.it

ABSTRACT

The role of structural and dynamical disorder in semiconductors is a topic of fundamental relevance because of its contribution to the spectral line shape of the photoluminescence, and it plays a major role in ruling the carrier transport properties at the band edge. In this regard, a class of semiconductors, i.e., halide perovskites, deeply investigated in the last decade, shows a peculiar degree of disorder, which has only been recently under investigation. The interest to study disorder in halide perovskites is related to the large set of innovative applications of this class of materials, spanning from energy harvesting to high brilliance incoherent and coherent light emitters. In this perspective, we show that quantitative information on the disorder in halide perovskites can be extracted by deep analysis of the photoluminescence in different experimental conditions. Our study, conducted on a large set of samples of a metal halide perovskite, $CsPbBr_3$, prepared with various synthesis/deposition methods, clarifies the relative weight of the static and dynamic contributions. A comparison with theoretical predictions is provided, gaining insights into the exciton/carrier–phonon interaction in metal halide perovskites.

I. INTRODUCTION

Since the seminal work of Protesescu *et al.*,[1] the inorganic cesium lead halide perovskites ($CsPbX_3$, X = Cl, Br, I) and their alloys have been considered emerging materials for optoelectronic and photovoltaic applications.[2] Their large color gamut ranging from deep blue to deep red is extremely appealing for many applications; indeed, $CsPbI_3$ has a red emission (1.7 eV), $CsPbBr_3$ has a green emission (2.3 eV), $CsPbCl_3$ has a blue emission (3 eV), and by varying the halogen composition, the entire UV-visible spectral range can be covered. Moreover, inorganic halide perovskites offer a superior stability under operation with respect to the analogous hybrid organic–inorganic perovskites, being the main problem the material decomposition in the presence of moisture and after long exposition to light. Even though inorganic perovskites show a much better stability and reduced aging with respect to the hybrid ones, further improvements are required to guarantee the aging time comparable to the most common semiconductors. Despite these perovskites are considered "defect tolerant,"[3–6] their defects are related not only to the presence of elements different from the constituent ones but also to structural disorders like vacancies, deviation from stoichiometry, domains formation, and lattice distortion, possibly combined with local strain. In fact, in perovskites,

especially in the inorganic ones, an additional distinction is needed between static structural disorder (i.e., vacancies, deviation from stoichiometry) and dynamic disorder arising from the lattice vibrations; it is worth noting that even though domains and lattice distortions are not completely static, they are not considered to provide a dynamic contribution to disorder. The dynamic disorder, intimately related to the structural instability of these perovskites[7–10] around room temperature, has been the object of several investigations, both experimental[11–13] and theoretical,[14–16] and, even if several aspects are still debated (i.e., the presence of a dynamical Rashba effect[17–19]), it certainly affects the carrier dynamics and the overall properties, as recently reported in two-dimensional lead halide perovskites.[20] As far as the carrier dynamics and the radiative efficiency are concerned, the disorder, independently from its nature, manifests itself mainly in two striking ways: a reduction of the carrier lifetime and mobility, with the consequent emission quenching, and a spectral broadening of the photoluminescence (PL) spectrum. While deep traps and recombination centers, arising from static disorder, affect only the lifetimes, the shallow states related to static and/or dynamic disorder influence both the carrier dynamics and the spectral shape. With the exception of a few single nanocrystals of outstanding quality that exhibit very long carrier lifetimes and mobility[21] and/or very narrow PL linewidths,[22,23] at low temperatures, most of the samples show lifetimes of the order of a few hundreds of ps and PL linewidths of few meVs.[24] Typically, the PL due to the exciton radiative recombination consists of the main peak and two tails, at higher and lower energy with respect to it. The low energy contribution is commonly reported as the Urbach tail (UT); its slope as well as the width of the main PL peak depends on the degree and nature of the disorder. Most of the studies of the Urbach tail in halide perovskites mainly addressed the close relation between UT and the overall performance of the material for photovoltaic applications.[25,26] In this perspective, we aim to provide a more general picture of the characteristics of the Urbach tail in inorganic halide perovskites and its relationship with the nature of the disorder. In particular, we analyze several samples of $CsPbBr_3$ grown with different techniques, namely *bulk* crystals, spin-coated (SC) thin films, and layers of nanometric thickness grown by radio-frequency (RF) magnetron sputtering (MS). By means of time-integrated (TI) and ps time-resolved (TR) PL measurements, as a function of the temperature and the excitation power, we elucidate the role of both dynamic and static disorders in the exciton/carrier recombination dynamics and in the spectral characteristics of $CsPbBr_3$, as well we highlight the role of strain in determining the bandgap energy.

II. EXPERIMENTAL

A large set of $CsPbBr_3$ samples were prepared and investigated: a macro-crystal (hereafter indicated as *bulk*) sample, with a mm size along each axis, was grown by the antisolvent vapor-assisted crystallization (AVC),[27] and methanol was used as antisolvent. As reported in Ref. 28, the macro-crystal shows the presence of a few differently oriented crystalline domains detected in the XRD pattern. Given the size of the excitation spot ($\approx 10^{-2}$ mm^2), which is smaller than the domain size, we can consider the response of the sample as that of a single crystal. Microcrystal ensembles were realized by spin-coating, on a soda lime glass (SLG) or silicon (Si) substrate, a $CsPbBr_3$ solution prepared by dissolving equal molar quantity of the precursors (CsBr and $PbBr_2$) in dimethyl sulfoxide.[29] The solution was stirred overnight to obtain a clear liquid. After the spinning, the samples were dried and annealed at 120 °C for 10 min. Thin films of $CsPbBr_3$ were also realized by radio-frequency magnetron sputtering with the procedure described in Ref. 30; several samples were investigated with thickness in the range 50–500 nm deposited on different substrates: here, we will present results on SLG and Si.

A full morphological and structural characterization of the different samples was done using several techniques [scanning electron microscopy (SEM), x-ray photoelectron spectroscopy (XPS), x-ray diffraction, and SNOM topography] and it can be found in Refs. 28, 30, and 31: it is only worth mentioning that the typical size of crystals in spin-coated and magnetosputtered samples ranges between few tens of nm to 1 μm, being the main difference between the two kinds of samples the homogeneity and compactness of the film. Moreover, all investigated samples do not show evident material decomposition/aging over months, keeping them in controlled dry ambient.

Photoluminescence experiments were realized with excitation/detection at macro-scale (macro-photoluminescence hereafter indicated as MPL) and micro-scale (microphotoluminescence hereafter indicated as μPL). Typically, in the MPL configuration, the excitation spot was 10^{-4} cm^2 while it was 1–2 μm^2 in the μPL setup. All MPL experiments were performed in a quasi-backscattering geometry, keeping the samples in a closed cycle cryostat and varying the temperature in the range 10–300 *K*. Microphotoluminescence experiments were realized by using a home-made confocal microscope equipped with a Mitutoyo 100x objective (378-806-3, NA = 0.7) or a Mitutoyo 50x objective (378-818-4, NA = 0.42), providing a spatial resolution of about 500 nm or 1 μm depending on the objective. Samples were kept in a low-vibration Janis ST-500 cryostat, which was mounted on a Physik Instrumente x–y translation stage for scanning the sample surface. The spectral resolution was $\leq$1 meV in both MPL and μPL experiments. A frequency-doubled mode-locked ps Ti-Sapphire laser, operating at 81.3 MHz repetition rate with 1.2 ps long pulses, was used for TR-PL experiments; in this case, the maximum excitation intensity was about 10 W/cm^2, corresponding to an estimated excitation density of about 2×10^{16} cm^{-3} carriers per pulse. TR-PL measurements were carried out only in the macro-scale configuration using a synchroscan streak camera (time resolution 5 ps) after spectral dispersion of the detected signal through a 25 cm monochromator, equipped with a 300 gr/mm (blaze 500 nm, spectral resolution 2 meV). It is worth mentioning that no change in the spectral features, in particular, on the Urbach tail, the focus of this work as discussed in Secs. III A and III B, was found afters tens of temperature cycles between 300 and 10 K.

III. RESULTS

A. CW PL

In Fig. 1, we report, in a log scale, the PL spectra of a $CsPbBr_3$ spin-coated film on SLG as a function of the temperature T under

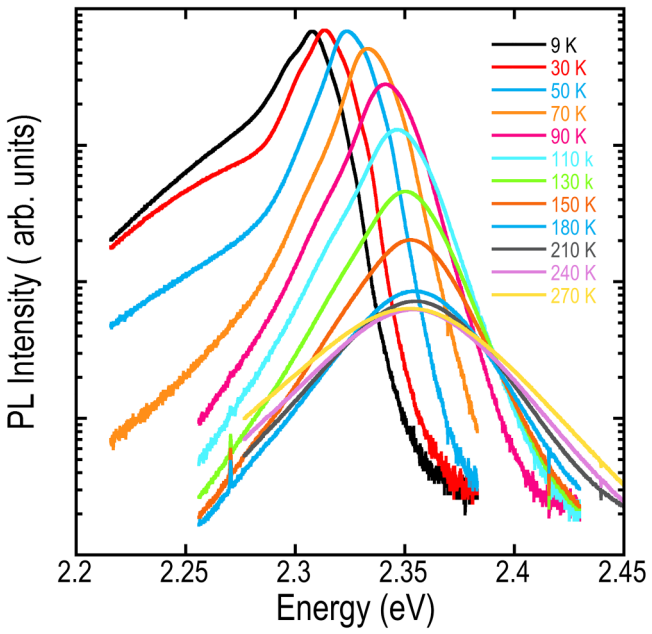

FIG. 1. PL spectra as a function of T for a $CsPbBr_3$ spin-coated film on a soda-lime glass substrate.

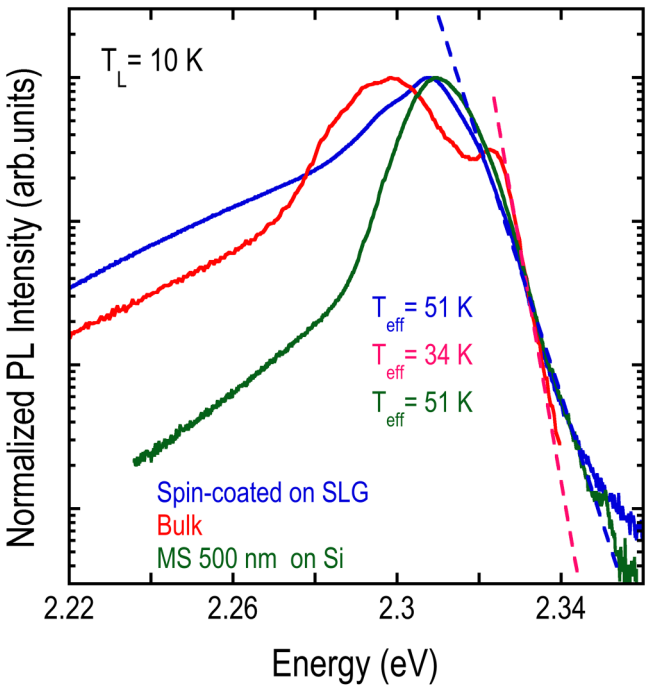

FIG. 2. Low temperature PL spectrum of different $CsPbBr_3$ samples: *bulk* sample (red curve), spin-coated thin film (blue curve), and 500 nm thick film obtained by RF-MS on silicon (green curve). The dashed lines are fits of the high energy tail and the effective temperatures are reported.

CW excitation at 405 nm (3.062 eV), well over the bandgap energy, with an excitation density of $\leq 10\,W/cm^2$.

As expected, the PL spectra, dominated by the exciton emission, exhibit a central peak and exponential tails. At low temperature, the PL peak has a central Gaussian shape with a shoulder on the low energy side, more or less pronounced depending on the sample, due to localized or bound exciton emission. Such Gaussian shape denotes the presence of disorder and the PL broadens with an increase in the temperature. The other two relevant features concern the presence of two nearly exponential tails, one in the high energy side and the other in the low energy side of the PL spectrum. The tail on the high energy side, whose slope changes with T, is often observed in the PL: it comes from the thermal distribution of the excitons and free carriers population. The contribution of the excitons in the high energy tail should be absent in a perfect semiconductor, and it originates from processes (i.e., disorder, impurity scattering, localization) that, breaking the wavevector K selection rule, allows radiative recombination of excitons with $K \neq 0$. The shape of the excitonic tail depends on several factors: the exciton density of states (DOS),[32] the K-vector indeterminacy, due to disorder, and the temperature that determines the population of the high energy states. In a non-degenerate condition, as in our experimental condition (low excitation density), the exciton population has a Boltzmann distribution giving rise to the slope of the high energy exponential tail that can be used to evaluate the temperature of the excitons. Assuming a complete relaxation of the K selection rule, in 2D systems, with a step-like density of states (DOS), this slope directly provides the temperature of the exciton gas. In 3D systems, with a DOS having a square root dependence on the energy, the slope gives an effective temperature T_{eff} no more than 10% higher than real excitonic temperature. In Fig. 2, we compare the PL spectra, normalized at the peak intensity, at low T for differently prepared samples. The PL of the *bulk* sample is dominated by the bound exciton emission at around 2.298 eV, while the free exciton emission is at 2.323 eV.[33] The bound exciton emission disappears with an increase in T. The sputtered and the spin coated films have a similar PL peak at 2.309 eV. All of them exhibit similar spectra with a high energy exponential tail, which corresponds to an exciton temperature T_{eff} higher than the lattice temperature T_L.

The higher exciton temperature with respect to the lattice is commonly and already found[28,34,35] at low T and gradually the two temperatures get equal at higher T. The mismatch between the lattice (T_L) and exciton (T_{eff}) temperature indicates the incomplete thermalization between the exciton gas and the phonon reservoir in the time scale of the exciton lifetime.[36] The low energy tail of PL in Fig. 2 is nearly bi-exponential at low T and rising T gradually becomes mono-exponential; this rather relevant tail in PL is related to the Urbach Tail (UT), so correlated to disorder, and it is the focus of our work.

First information on the nature of disorder can be obtained by the behavior of the PL spectra with varying excitation densities.

In Fig. 3, we show the change in the spectra of a spin coated sample at a lattice temperature of 10 K varying the incident power over four orders of magnitude (30 nW–1 mW). At the lowest

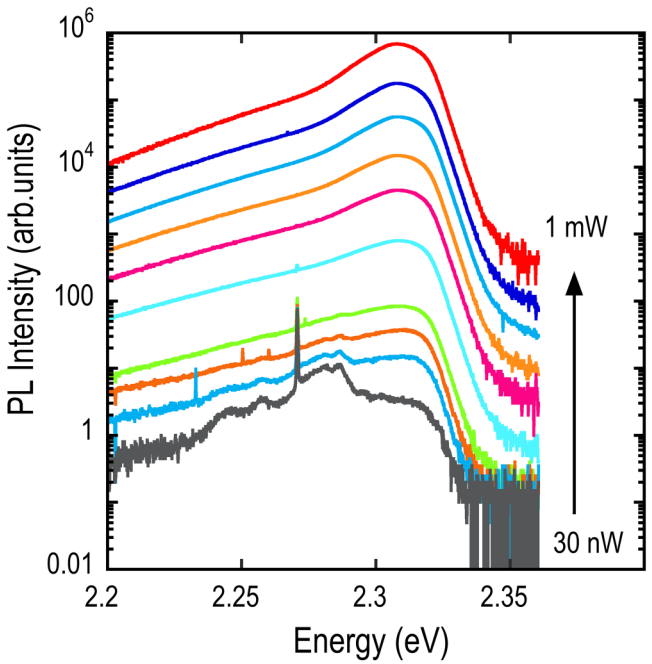

FIG. 3. Low temperature PL spectra of a spin-coated $CsPbBr_3$ sample on a Si substrate as a function of the excitation power. The step in the power follows the sequence 1-3-10.

power, the PL is dominated by defects and the excitonic contribution is rather scarce. Increasing the excitation density, the emission arising from defects saturates and the excitonic contribution to PL becomes progressively dominant; at the same time, the low energy tail experiences an analogous growth and acquires an exponential constant slope, thus evidencing a close correlation with the exciton emission.

Provided that all the samples exhibit a certain degree of disorder, it is important to determine the extent of their spatial inhomogeneity, determined by the static component of the disorder. With this respect, μPL at low T can provide a distinction between disorder acting on a macroscale, i.e., over lengths exceeding a micrometer, or on a submicrometer scale. In Fig. 4, a comparison at 10 K is shown between the PL of the *bulk* sample (a) and a spin-coated film on SLG (b) detected with the macro-PL setup compared with a set of measurements in different points of the samples detected by the confocal μPL setup.

For the *bulk* sample, it comes out that the bound exciton emission at around 2.3 eV and the free exciton emission at 2.32 eV show a very similar broadening irrespective of the spatial scale of the detection setup, indicating that this broadening originates from a disorder on a submicrometer length scale. Moreover, the static disorder is responsible for the different weight in PL of the free exciton line with respect to the bound exciton emission in different sample regions as shown in Fig. 4(a). Most likely, this emission arises from excitons bound to vacancies[3,33] and, as expected, it disappears with an increase in the lattice temperature. Therefore, the observed changes in its intensity are not surprising as we change the detection spot. In the case of the spin-coated sample [Fig. 4(b)], slight differences are found concerning the exciton energy with no major change in the PL line shape, evidence again of a disorder on a spatial scale less than one μm. The graph in log scale helps in showing the very same characteristics of the low energy tail, irrespective of the detection (macro-PL/μPL).

In the presence of a relevant contribution of static disorder, we expect to detect changes in the low energy tail, depending on the excited spot in the sample. On the contrary, as shown in Fig. 4,

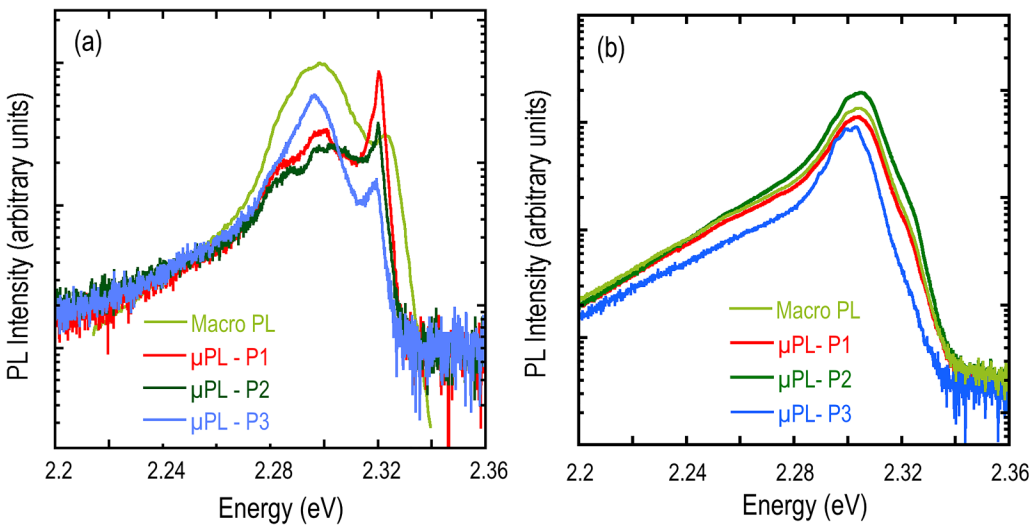

FIG. 4. Comparison between μPL (1 μm spot) and macro-PL spectra (100 μm spot) at a lattice temperature of 10 K for the *bulk* sample (a) and for a spin-coated sample on SLG (b). P1, P2, and P3 are different points of the samples.

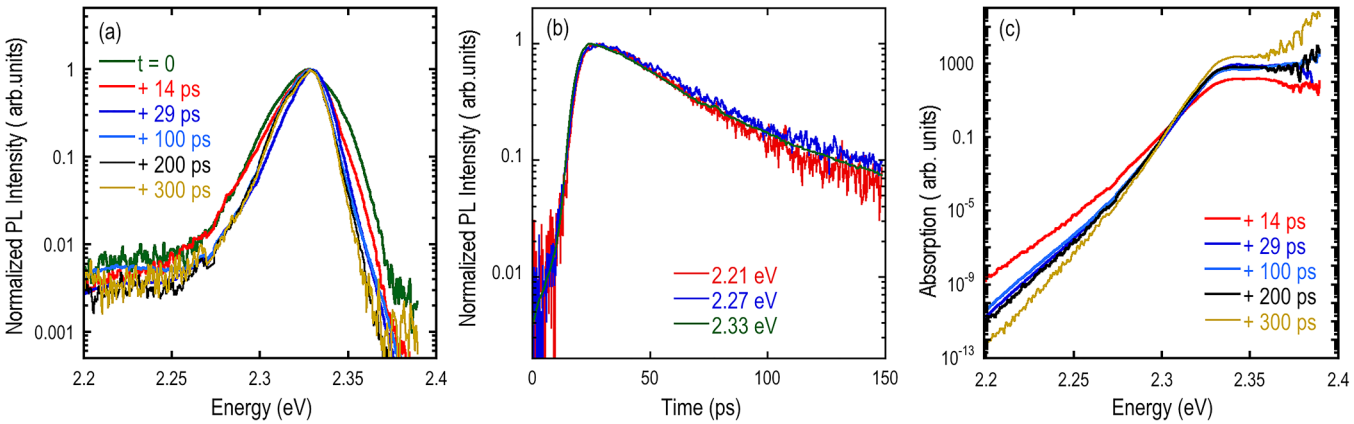

FIG. 5. (a) Time resolved PL spectra at $T_L = 10$ K of a 70 nm thick film deposited on SLG by means of RF-MS. (b) PL decays at two energies in the Urbach tail and at the exciton energy. (c) Absorption extracted from (a) as discussed in the text.

the absence of major modifications of the low energy exponential component of the PL is a result supporting the negligible contribution of the static disorder in the Urbach tail.

B. TR PL

More information on the kind of disorder, static and dynamic, at the origin of the Urbach tail can be obtained by time resolved (TR) PL. In fact, in CW PL measurements, static and dynamic disorder give rise to very similar features. Instead, TR PL spectra, giving direct access to the population dynamics of the states contributing to the radiative emission, can elucidate the different nature of disorder. In particular, on a picosecond time scale, an exponential tail due to dynamic disorder, closely related to the exciton-phonon interaction, is expected to follow the exciton dynamics without relevant changes in the spectral shape. On the contrary, the carrier thermalization inside an exponential tail of real states, originating from static disorder, typically occurs on the scale of several tens of ps giving rise to different time evolutions inside the PL band. In fact, the exciton and carrier localization typically produces a characteristic spectral diffusion[37,38] and a marked variation of the dynamics inside the PL band, as also observed in the PL rise time/decay time at different energies inside the PL spectrum.[28]

In Fig. 5(a), normalized TR PL spectra are shown for a 70 nm thick sample prepared by RF magnetron sputtering on SLG. In the high energy side, an exponential tail clearly appears with a slope decreasing with time delay as a consequence of the exciton gas cooling whose temperature gradually approaches that of the lattice, as extensively discussed in Ref. 28. The complete thermalization of the excitons shows up with a constant slope of the high energy PL exponential tail. Concerning the time evolution of the low energy side of the PL, we underline the absence of an internal dynamics and a decrease of the exponential slope during the excitons cooling until their temperature gets stabilized. Therefore, the same dynamics, as shown in Fig. 5(b) for different energies, i.e., the exciton and two energies in the low energy side, characterizes the Urbach tail and the exciton emission, and this is the signature of the intrinsic nature of the Urbach tail, arising from a dynamic disorder.

IV. DISCUSSION

As previously shown, the investigated samples show spatial inhomogeneity which, in the case of the *bulk* sample shown in Fig. 4, mainly affects the relative contribution of the free exciton and bound exciton emission and does not produce any relevant change in the free exciton linewidth and in the low energy tail. In the spin coated and sputtered samples, the PL detected at a macro-scale with respect to that at a micro-scale shows only a few meVs (nearly 2 meV) increase in the line broadening with no change in the shape. Then, in all the samples, at low temperature we observe a limited randomness of the free exciton energy on a macro-scale, the main broadening occurring on sub-micrometer scale as a result of a static disorder.

Moreover, we have shown that in both CW and TR experiments the excitons and carriers population get thermalized in a few ps. The presence of a thermalized distribution at a temperature T_{eff}, higher than the lattice one at low T and gradually approaching this latter rising T, allows to extract the absorption $\alpha(E)$ from PL spectra given the relation[39,40]

$$I_{PL}(E) = E^2\alpha(E)e^{-\frac{E}{KT_{eff}}}, \quad (1)$$

where $\alpha(E)$ is the absorption coefficient and T_{eff} is the effective temperature of the excitons/carriers population as extracted from the high energy tail of the PL spectrum. Given the low excitation density used in our experiment $\leq 10^{16}\,\mathrm{cm}^{-3}$, we are in a non-degenerate case and we can therefore assume a Boltzmann distribution. We want to remark that in several cases the direct measurement of the absorption coefficient and, in particular, its spectral dispersion is a difficult task, for nanometric thin films or for thick samples, and when the substrate is an absorbing material unless to resort to techniques as etching. Therefore, the

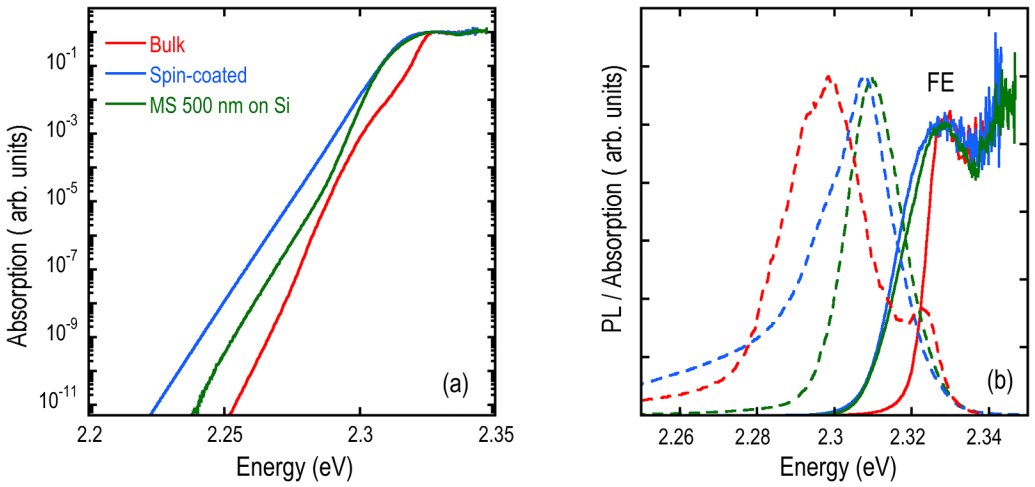

FIG. 6. (a) Absorption in log scale as extracted from PL spectra of Fig. 2 and (b) PL spectra of Fig. 2 in linear scale (dashed lines) and absorption (continuous lines) in linear scale.

use of the PL spectrum is a very efficient way to retrieve $\alpha(E)$, having a high sensitivity so to cover an extended dynamic range as shown below.

According to Eq. (1) $\alpha(E)$ extracted from the spectra of Fig. 2 is shown in Fig. 6. Using a log scale representation [Fig. 6(a)], we can appreciate the extended UT over ten orders of magnitude, while in linear scale [Fig. 6(b)] the free exciton resonance is visible and the Stokes Shift (SS) of the PL (dashed lines) with respect to the absorption can be observed.

As previously discussed, the hypothesis of thermal equilibrium has to be verified for TR experiments. If we exclude the first few picoseconds needed to the exciton gas to reach a quasi-equilibrium thermal distribution, characterized by a temperature T_{eff} , typically higher than T_L,[28] we can extract the absorption considering a fully thermalized regime. In Fig. 5(c), we show the absorption as extracted from the spectra of Fig. 5(a) at different time delays: in the considered time interval, the effective excitonic temperature changes from 81 K (delay +14 ps) to 51 K (delay $\geq$300 ps). Quite remarkable is the presence of the exponential tail covering more than ten orders of magnitude and whose slope follows the decrease of T_{eff}, denoting the strong correlation between such slope and the exciton dynamics. This is a clear evidence of the intrinsic nature of the Urbach tail, related to the dynamic disorder due to the exciton–phonon interaction, being negligible the contribution of the static disorder.

In Fig. 7, the absorption of the spin coated sample on soda lime glass is determined at different temperatures as extracted from PL spectra of Fig. 1.

From the exponential tail covering several orders of magnitude, we extract the value of the Urbach energy E_U. In addition, provided that in disordered systems the PL peak energy, due to the Stokes shift, does not give directly the exciton energy E_b, we have estimated this latter in an approximated way. Without recurring to a rather complicated PL fit, we have evaluated, for each temperature, E_b^* as the energy of the intercept, on a log scale, of the line determined by the almost horizontal DOS and the line determined by the exponential tail, as shown in Fig. 7(b). Provided that the shift of E_b^* with respect to the exciton energy E_b is independent of T, i.e., from E_U, there is no loss in generality assuming $E_b = E_b^*$ as long as we are interested to its variation with T. In Fig. 8, the Urbach energy E_U and E_b are reported as a function of the lattice temperature for the whole set of investigated samples.

While the Urbach energy E_U increases monotonously with T_L, and almost linearly at high T, the dependence of E_b on T_L changes around 100–150 K, showing a marked flattening as commonly reported in the literature. This latter behavior, which turns out to be sample dependent, highlights that other processes, in addition to the intrinsic ones due to the exciton–phonon interaction, play a role in determining the temperature dependence of the bandgap energy.

Similar results are found for all the investigated samples; in Fig. 9, the relationship between the value of the energy E_b and the Urbach energy E_U is reported for each temperature.

All samples show similar behavior in the temperature range 10–270 K; in particular, apart from the *bulk*, the same dependence of E_b on E_U, almost linear, is found at low T, below $T_M \approx 110$ K. Instead, above T_M, the relation between E_b and E_U deviates from linearity in a sample-dependent way. Quite remarkable is also the fact that similar values of the Urbach energy, as the ones here found, are reported in the literature for halide perovskites nanocrystals and quantum dots,[26,41,42] suggesting that the origin of the tail in this class of materials does not involve relevant contribution from the crystal surfaces.

To understand the experimental findings, we have to consider that the exciton/carrier–phonon interaction is responsible for the bandgap shift with T, as a consequence of the T-dependent phonon occupation number n, and it also accounts for the increase in the Urbach tail slope due to its growing fluctuation with T. Having both processes the same dependence on n, Cody and other

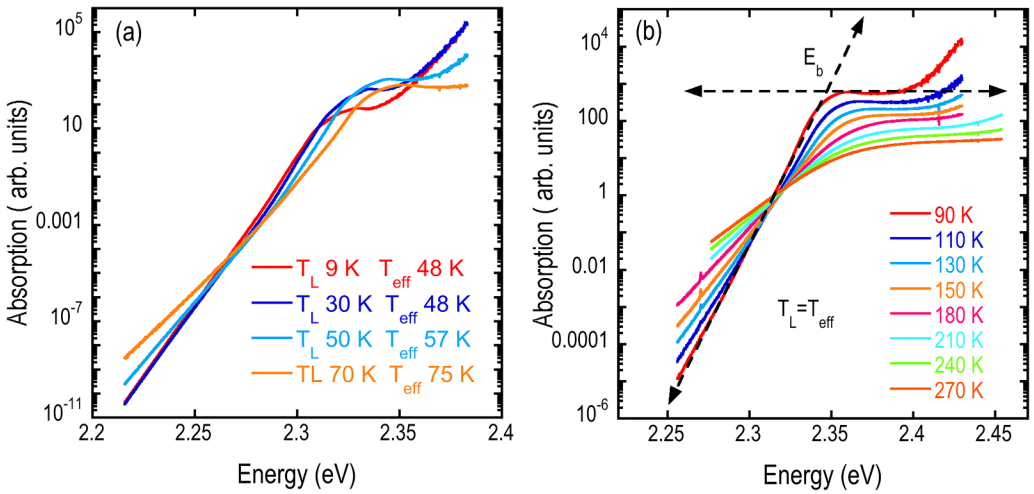

FIG. 7. Absorption as a function of T: (a) low T range and (b) high T range.

researchers[43,44] stated an almost linear dependence of E_b on E_U if the same phonons are involved, which in our case explains the results of Fig. 9 below T_M. For temperature $T \geq T_M$, we find a behavior that cannot be reproduced by a competition between phonon modes as already invoked in Ref. 45, and it is rather sample dependent. It has to be noted that the lattice thermal expansion accounts only in part to the bandgap energy shift. In fact, on the basis of the few experimental data at room temperature concerning the volumetric expansion coefficient α , the bulk modulus B,[46] and the pressure coefficient of the bandgap,[47] we can estimate a value of $\frac{dE_g}{dT} = 5.84 \times 10^{-2}$ meV/K at room T. Even considering the variation of α with T, in the framework of the Einstein–Debye model with a phonon energy of 12 meV, the estimated change in the bandgap energy is around 14 meV in the range 10–300 K (with a negligible dependence on the phonon energy) not accounting for the results of Fig. 8(b). Moreover, above 50 K, the energy shift of the bandgap due to the lattice expansion results linear, again very different from the data of Fig. 8(b). Therefore, the experimental findings of Figs. 8(b) and 9 can be ascribed to an extrinsic mechanism like a release of the strain in the bulk of the crystal or at the interface between the film and the substrate.

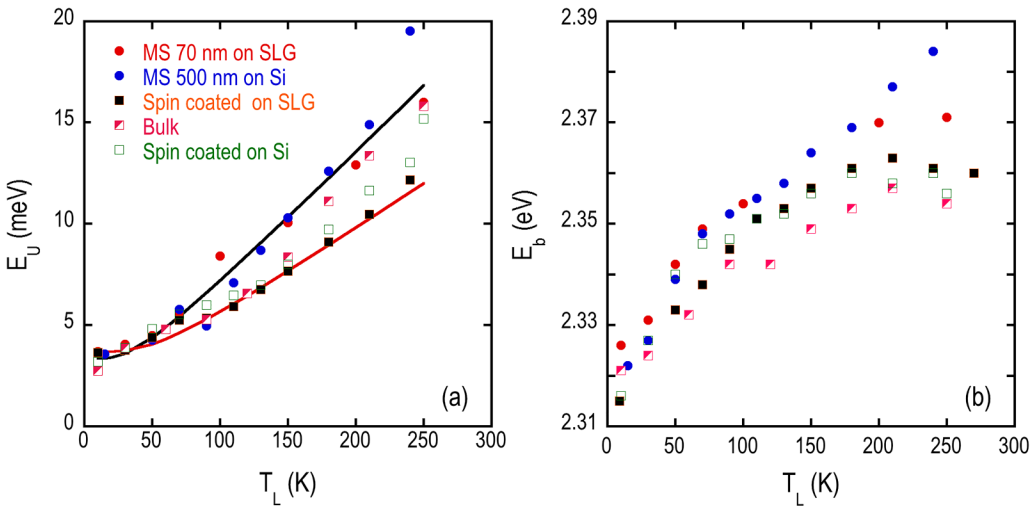

FIG. 8. (a) E_U vs T_L for the whole set of investigated samples. The solid lines are fits as discussed in the text. (b) E_b vs T_L for the whole set of investigated samples.

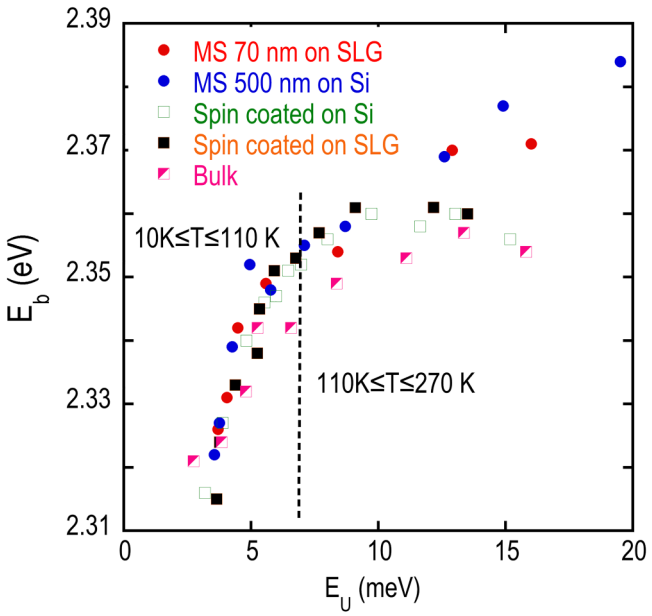

FIG. 9. Dependence of E_b on E_U for samples differing for substrate, thickness, and synthesis/deposition method. The dashed line separates the temperature range below/above 110 K.

The experimental data of Fig. 8(a) can be reproduced according to the expression reported by Cody *et al.*,[43]

$$E_U = \frac{\hbar\omega_{ph}}{\sigma_0}\left[\frac{(1+X)}{2} + \frac{1}{\exp(\hbar\omega_{ph}/k_BT)-1}\right], \quad (2)$$

where $\hbar\omega_{ph}$ is the average phonon energy, σ_0 is the steepness parameter, and X is the static disorder contribution normalized to zero-point fluctuations. The solid lines in Fig. 8(a) are two different fits with the same X value of 0.01, and two different values of the average phonon energy, and steepness parameter; the black (red) line corresponds to $\hbar\omega_{ph} = 9$ (13) meV, in agreement with the phonon energies in $CsPbBr_3$[48,49] and $\sigma_0 = 1.3(1.8) \times 10^{-3}$, respectively. The other experimental data can be fitted with values of $\hbar\omega_{ph}$ and σ_0 intermediates between them and the same value for X.

The experimental results previously shown bring clear evidence that in $CsPbBr_3$ the Urbach tail has an intrinsic origin, related to the exciton–phonon interaction, and that the contribution of the static disorder is quite small. Being the values of the Urbach energy reported in the literature[25,26] for other types of halide perovskites comparable to the ones here discussed, we believe that the intrinsic nature of the Urbach tail is a common characteristic of this class of materials. Different models have been proposed for the dependence of E_U on temperature in semiconductors. An exciton self-trapping has been considered in the presence of a strong exciton–phonon interaction as in Ref. 50. The fluctuations of the band edge due to thermal phonons have been addressed as the origin of the Urbach tail in Ref. 44. Finally, the electric field at the micro-scale due to phonon thermal excitation has been discussed in Ref. 51. In all these theoretical frameworks, the dependence of E_U on T is the same as in Ref. 43 and Eq. (2) making the identification of a specific mechanism very hard.

In conclusion, the experimental data collected in a variety of samples differing for growth condition and morphology evidence a common trend as far as the temperature dependence of the bandgap and the disorder are concerned. All the samples exhibit a more or less relevant effect due to the strain when moving toward room temperature that unavoidably will give rise to an increase in the spatial inhomogeneity. Nevertheless, the effects on the Urbach exponential tail seem to be negligible as this one turns out to be determined by the intrinsic mechanism rather than the static disorder that, at low T, gives rise, below E_b, to an exponential density of states with a steep slope around 0.2 meV.

Given the impressive advances in optoelectronics based on halide perovskites in the last decade, it is of interest to comment if the UT can represent a limitation to the performance of a device. In fact, if the UT comes from intragap states that eventually affect the transport mechanism and the carrier recombination, the impact on a device efficiency is undoubt. Instead, on the basis of the results here discussed and literature data, we can conclude that in halide perovskites the presence of the Urbach tail will not represent a limit to the performance of a solar cell or a light emitting device, which are presently the most interesting devices under study. In fact, investigations on the correlation between the UT and the photovoltaic conversion efficiency[25,52] and recent results[53,54] bring to the conclusion that, on one side the intrinsic origin of UT can explain the large values of the open circuit voltage in solar cells, and, on the other side, the limitation in power conversion efficiency comes from the high content of defects at the interfaces between the active layer and the charge transport layer (CTL), so requiring a proper engineering of such interfaces.[53,54] Again, in halide-perovskites LEDs, the overall performance has been improved by material engineering[55] (controlling the grain size, optimizing the injection of carriers, etc.); presently, the major problem seems to rely on the light extraction efficiency due to the large refractive index mismatch so that photonic structures have been recently used to improve the external efficiency.[56]

V. CONCLUSIONS

We have presented a study on the nature of the Urbach tail in an inorganic halide perovskite, $CsPbBr_3$, but, provided that also hybrid halide perovskites show a similar behavior as reported in the literature, we are confident that our analysis can be extended to the whole class of these semiconductors. The experimental findings on a large set of samples, prepared with different synthesis/deposition methods, indicate a very similar behavior independent of the sample morphology (*bulk*, thin nanocrystalline films), thickness, substrate, and growth/deposition technique. Our results indicate that the Urbach tail has an origin ascribable to the dynamic disorder, induced by the lattice vibrations, which in a limited temperature range is linearly correlated to the bandgap variation and the exciton energy E_b. While the dependence of E_U on T nicely follows the phonon population, the discrepancy observed for E_b from the

expected intrinsic contribution, being strongly sample-dependent, has to be ascribed to an extrinsic phenomenology possibly related to strain release between grains in macro-crystal samples and between substrate and film in spin-coated and sputtered samples.

ACKNOWLEDGMENTS

The authors thank F. Bogani for helpful discussion and comments and S. Caporali for suggestions in the sample preparation.

AUTHOR DECLARATIONS

Conflict of Interest

The authors have no conflicts to disclose.

Author Contributions

A.V. conceived and designed the experiments. N.F., G.R., and A.V. performed the MPL experiments. A.R. and F.B. performed the μPL experiments. N.C. prepared the samples. N.F. and A.V. wrote the manuscript. All the authors contributed to manuscript editing.

DATA AVAILABILITY

The data that support the findings of this study are available from the corresponding author upon reasonable request.

REFERENCES

[1]L. Protesescu, S. Yakunin, M. I. Bodnarchuk, F. Krieg, R. Caputo, C. H. Hendon, R. X. Yang, A. Walsh, and M. V. Kovalenko, "Nanocrystals of cesium lead halide perovskites ($CsPbX_3$, X = Cl, Br and I): Novel optoelectronic materials showing bright emission with wide color gamut," Nano Lett. **15**, 3692–3696 (2015).

[2]X. Li, F. Cao, D. Yu, J. Chen, Z. Sun, Y. Shen, Y. Zhu, L. Wang, Y. Wei, Y. Wu, and H. Zeng, "All inorganic halide perovskites nanosystem: Synthesis, structural features, optical properties and optoelectronic applications," Small **13**, 1603996 (2017).

[3]J. Kang and L.-W. Wang, "High defect tolerance in lead halide perovskite $CsPbBr_3$," J. Phys. Chem. Lett. **8**, 489–493 (2017).

[4]M. Bruzzi, F. Gabelloni, N. Calisi, S. Caporali, and A. Vinattieri, "Defective states in micro-crystalline $CsPbBr_3$ and their role on photoconductivity," Nanomaterials **9**, 177 (2019).

[5]M. Bruzzi, N. Falsini, N. Calisi, and A. Vinattieri, "Electrically active defects in polycrystalline and single crystal metal halide perovskite," Energies **13**, 1643 (2020).

[6]F. Biccari, N. Falsini, M. Bruzzi, F. Gabelloni, N. Calisi, and A. Vinattieri, "Defects in perovskites for solar cells and LEDs," in *Defects in Functional Materials* (World Scientific Publishing, Singapore, 2020), Chap. 3, pp. 49–91.

[7]D. B. Straus, S. Guo, A. M. Abeykoon, and R. J. Cava, "Understanding the instability of the halide perovskite $CsPbI_3$ through temperature-dependent structural analysis," Adv. Mater. **32**, 2001069 (2020).

[8]J. Jiang, F. Liu, I. Tranca, Q. Shen, and S. Tao, "Atomistic and electronic origin of phase instability of metal halide perovskites," ACS Appl. Energy Mater. **3**, 11548–11558 (2020).

[9]M. Kirschner, B. Diroll, P. Guo, S. Harvey, W. Helweh, N. Flanders, A. Brumberg, N. Watkins, A. Leonard, A. Evans, M. Wasielewski, W. Dichtel, X. Zhang, L. Chen, and R. Schaller, "Photoinduced, reversible phase transitions in all-inorganic perovskite nanocrystals," Nat. Commun. **10**, 504 (2019).

[10]R. X. Yang, J. M. Skelton, E. L. da Silva, J. M. Frost, and A. Walsh, "Spontaneous octahedral tilting in the cubic inorganic cesium halide perovskites $CsSnX_3$ and $CsPbX_3$ (X = F, Cl, Br, I)," J. Phys. Chem. Lett. **8**, 4720–4726 (2017).

[11]K. T. Munson, E. R. Kennehan, G. S. Doucette, and J. B. Asbury, "Dynamic disorder dominates delocalization, transport, and recombination in halide perovskites," Chem **4**, 2826–2843 (2018).

[12]A. M. A. Leguy, A. R. Goñi, J. M. Frost, J. Skelton, F. Brivio, X. Rodríguez-Martínez, O. J. Weber, A. Pallipurath, M. I. Alonso, M. Campoy-Quiles, M. T. Weller, J. Nelson, A. Walsh, and P. R. F. Barnes, "Dynamic disorder, phonon lifetimes, and the assignment of modes to the vibrational spectra of methylammonium lead halide perovskites," Phys. Chem. Chem. Phys. **18**, 27051–27066 (2016).

[13]L. Piveteau, M. Aebli, N. Yazdani, M. Millen, L. Korosec, F. Krieg, B. M. Benin, V. Morad, C. Piveteau, T. Shiroka, A. Comas-Vives, C. Copéret, A. M. Lindenberg, V. Wood, R. Verel, and M. V. Kovalenko, "Bulk and nanocrystalline cesium lead-halide perovskites as seen by halide magnetic resonance," ACS Cent. Sci. **6**, 1138–1149 (2020).

[14]C. Gehrmann and D. Egger, "Dynamic shortening of disorder potentials in anharmonic halide perovskites," Nat. Commun. **10**, 3141 (2019).

[15]M. J. Schilcher, P. J. Robinson, D. J. Abramovitch, L. Z. Tan, A. M. Rappe, D. R. Reichman, and D. A. Egger, "The significance of polarons and dynamic disorder in halide perovskites," ACS Energy Lett. **6**, 2162–2173 (2021).

[16]M. J. Schilcher, P. J. Robinson, D. J. Abramovitch, L. Z. Tan, A. M. Rappe, D. R. Reichman, and D. A. Egger, "The significance of polarons and dynamic disorder in halide perovskites," ACS Energy Lett. **6**, 2162–2173 (2021).

[17]E. Mosconi, T. Etienne, and F. De Angelis, "Rashba band splitting in organohalide lead perovskites: Bulk and surface effects," J. Phys. Chem. Lett. **8**, 2247–2252 (2017).

[18]M. Isarov, L. Z. Tan, M. I. Bodnarchuk, M. V. Kovalenko, A. M. Rappe, and E. Lifshitz, "Rashba effect in a single colloidal $CsPbBr_3$ perovskite nanocrystal detected by magneto-optical measurements," Nano Lett. **17**, 5020–5026 (2017).

[19]B. Wu, H. Yuan, Q. Xu, J. Steele, D. Giovanni, P. Puech, J. Fu, Y. Ng, N. Jamaludin, A. Solanki, S. Mhaisalkar, N. Mathews, M. Roeffaers, M. Grätzel, J. Hofkens, and T. Sum, "Indirect tail states formation by thermal-induced polar fluctuations in halide perovskites," Nat. Commun. **10**, 484 (2019).

[20]W. Tao, C. Zhang, Q. Zhou, Y. Zhao, and H. Zhu, "Momentarily trapped exciton polaron in two-dimensional lead halide perovskites," Nat. Commun. **12**, 1400 (2021).

[21]Y. He, L. Matei, H. Jung, K. McCall, M. Chen, C. Stoumpos, Z. Liu, J. Peters, D. Chung, B. Wessels, M. Wasielewski, V. Dravid, A. Burger, and M. Kanatzidis, "High spectral resolution of gamma-rays at room temperature by perovskite $CsPbBr_3$ single crystals," Nat. Commun. **9**, 1609 (2018).

[22]M. Fu, P. Tamarat, H. Huang, J. Even, A. L. Rogach, and B. Lounis, "Neutral and charged exciton fine structure in single lead halide perovskite nanocrystals revealed by magneto-optical spectroscopy," Nano Lett. **17**, 2895–2901 (2017).

[23]J. Ramade, L. M. Andriambariarijaona, V. Steinmetz, N. Goubet, L. Legrand, T. Barisien, F. Bernardot, C. Testelin, E. Lhuillier, A. Bramati, and M. Chamarro, "Fine structure of excitons and electron–hole exchange energy in polymorphic $CsPbBr_3$ single nanocrystals," Nanoscale **10**, 6393–6401 (2018).

[24]G. Rainò, G. Nedelcu, L. Protesescu, M. I. Bodnarchuk, M. V. Kovalenko, R. F. Mahrt, and T. Stöferle, "Single cesium lead halide perovskite nanocrystals at low temperature: Fast single-photon emission, reduced blinking, and exciton fine structure," ACS Nano **10**, 2485–2490 (2016).

[25]S. De Wolf, J. Holovsky, S.-J. Moon, P. Löper, B. Niesen, M. Ledinsky, F.-J. Haug, J.-H. Yum, and C. Ballif, "Organometallic halide perovskites: Sharp optical absorption edge and its relation to photovoltaic performance," J. Phys. Chem. Lett. **5**, 1035–1039 (2014).

[26]M. Ledinsky, T. Schönfeldová, J. Holovský, E. Aydin, Z. Hájková, L. Landová, N. Neyková, A. Fejfar, and S. De Wolf, "Temperature dependence of the urbach energy in lead iodide perovskites," J. Phys. Chem. Lett. **10**, 1368–1373 (2019).

[27]J. Yu, G. Liu, C. Chen, Y. Li, M. Xu, T. Wang, G. Zhao, and L. Zhang, "Perovskite $CsPbBr_3$ crystals: Growth and applications," J. Mater. Chem. C **8**, 6326–6341 (2020).

[28]F. Gabelloni, F. Biccari, N. Falsini, N. Calisi, S. Caporali, and A. Vinattieri, "Long-living nonlinear behavior in $CsPbBr_3$ carrier recombination dynamics," Nanophotonics **8**, 1447–1455 (2019).

[29]D. Huang, P. Xie, Z. Pan, H. Rao, and X. Zhong, "One-step solution deposition of $CsPbBr_3$ based on precursor engineering for efficient all-inorganic perovskite solar cells," J. Mater. Chem. A **7**, 22420–22428 (2019).
[30]C. Borri, N. Calisi, E. Galvanetto, N. Falsini, F. Biccari, A. Vinattieri, G. Cucinotta, and S. Caporali, "First proof-of-principle of inorganic lead halide perovskites deposition by magnetron-sputtering," Nanomaterials **10**, 60 (2019).
[31]N. Falsini, A. Ristori, F. Biccari, N. Calisi, G. Roini, P. Scardi, S. Caporali, and A. Vinattieri, "A new route for caesium lead halide perovskite deposition," J. Eur. Opt. Soc. Rapid Publ. **17**, 8 (2021).
[32]R. F. Schnabel, R. Zimmermann, D. Bimberg, H. Nickel, R. Lösch, and W. Schlapp, "Influence of exciton localization on recombination line shapes: $In_xGa_{1-x}As/GaAs$ quantum wells as a model," Phys. Rev. B **46**, 9873–9876 (1992).
[33]M. Sebastian, J. A. Peters, C. C. Stoumpos, J. Im, S. S. Kostina, Z. Liu, M. G. Kanatzidis, A. J. Freeman, and B. W. Wessels, "Excitonic emissions and above-band-gap luminescence in the single-crystal perovskite semiconductors $CsPbBr_3$ and $CsPbCl_3$," Phys. Rev. B **92**, 235210 (2015).
[34]M. Gurioli, A. Vinattieri, J. Martinez-Pastor, and M. Colocci, "Exciton thermalization in quantum-well structures," Phys. Rev. B **50**, 11817–11826 (1994).
[35]Y. Yang, D. Ostrowski, R. France, K. Zhu, J. Van De Lagemaat, J. Luther, and M. Beard, "Observation of a hot-phonon bottleneck in lead-iodide perovskites," Nat. Photonics **10**, 53–59 (2016).
[36]F. Sekiguchi, H. Hirori, G. Yumoto, A. Shimazaki, T. Nakamura, A. Wakamiya, and Y. Kanemitsu, "Enhancing the hot-phonon bottleneck effect in a metal halide perovskite by terahertz phonon excitation," Phys. Rev. Lett. **126**, 077401 (2021).
[37]R. Singh, M. Richter, G. Moody, M. E. Siemens, H. Li, and S. T. Cundiff, "Localization dynamics of excitons in disordered semiconductor quantum wells," Phys. Rev. B **95**, 235307 (2017).
[38]H. He, Q. Yu, H. Li, J. Li, J. Si, Y. Jin, N. Wang, J. Wang, J. He, X. Wang, Y. Zhang, and Z. Ye, "Exciton localization in solution-processed organolead trihalide perovskites," Nat. Commun. **7**, 10896 (2016).
[39]R. Bhattacharya, B. Pal, and B. Bansal, "On conversion of luminescence into absorption and the van Roosbroeck-Shockley relation," Appl. Phys. Lett. **100**, 222103 (2012).
[40]T. Yamada, T. Handa, Y. Yamada, and Y. Kanemitsu, "Light emission from halide perovskite semiconductors: Bulk crystals, thin films, and nanocrystals," J. Phys. D: Appl. Phys. **54**, 383001 (2021).
[41]F. Liu, Y. Zhang, C. Ding, S. Kobayashi, T. Izuishi, N. Nakazawa, T. Toyoda, T. Ohta, S. Hayase, T. Minemoto, K. Yoshino, S. Dai, and Q. Shen, "Highly luminescent phase-stable $CsPbI_3$ perovskite quantum dots achieving near 100% absolute photoluminescence quantum yield," ACS Nano **11**, 10373–10383 (2017).
[42]S. Hou, M. K. Gangishetty, Q. Quan, and D. N. Congreve, "Efficient blue and white perovskite light-emitting diodes via manganese doping," Joule **2**, 2421–2433 (2018).
[43]G. D. Cody, T. Tiedje, B. Abeles, B. Brooks, and Y. Goldstein, "Disorder and the optical-absorption edge of hydrogenated amorphous silicon," Phys. Rev. Lett. **47**, 1480–1483 (1981).
[44]T. Skettrup, "Urbach's rule derived from thermal fluctuations in the band-gap energy," Phys. Rev. B **18**, 2622–2631 (1978).
[45]M. Cardona and R. Kremer, "Temperature dependence of the electronic gaps of semiconductors," Thin Solid Films **571**, 680–683 (2014).
[46]Y. Rakita, S. Cohen, N. Kedem, G. Hodes, and D. Cahen, "Mechanical properties of $APbX_3$ (A = Cs or CH_3NH_3; X = I or Br) perovskite single crystals," MRS Commun. **5**, 623–629 (2015).
[47]G. Xiao, Y. Cao, G. Qi, L. Wang, C. Liu, Z. Ma, X. Yang, Y. Sui, W. Zheng, and B. Zou, "Pressure effects on structure and optical properties in cesium lead bromide perovskite nanocrystals," J. Am. Chem. Soc. **139**, 10087–10094 (2017).
[48]M. Liao, B. Shan, and M. Li, "In situ raman spectroscopic studies of thermal stability of all-inorganic cesium lead halide ($CsPbX_3$, X = Cl, Br, I) perovskite nanocrystals," J. Phys. Chem. Lett. **10**, 1217–1225 (2019).
[49]S. Ghosh, D. Rana, B. Pradhan, P. Donfack, J. Hofkens, and A. Materny, "Vibrational study of lead bromide perovskite materials with variable cations based on raman spectroscopy and density functional theory," J. Raman Spectrosc. **52**, 2338 (2021).
[50]H. Sumi and Y. Toyozawa, "Urbach-Martienseen rule and exciton trapped momentarily by lattice vibrations," J. Phys. Soc. Jpn. **31**, 342–358 (1971).
[51]J. D. Dow and D. Redfield, "Toward a unified theory of Urbach's rule and exponential absorption edges," Phys. Rev. B **5**, 594–610 (1972).
[52]J. Wong, S. T. Omelchenko, and H. A. Atwater, "Impact of semiconductor band tails and band filling on photovoltaic efficiency limits," ACS Energy Lett. **6**, 52–57 (2021).
[53]U. K. Thakur, P. Kumar, S. Gusarov, A. E. Kobryn, S. Riddell, A. Goswami, K. M. Alam, S. Savela, P. Kar, T. Thundat, A. Meldrum, and K. Shankar, "Consistently high V_{oc} values in p-i-n type perovskite solar cells using Ni^{3+}-doped NiO nanomesh as the hole transporting layer," ACS Appl. Mater. Interfaces **12**, 11467–11478 (2020).
[54]H. Min, D. Lee, J. Kim, G. Kim, K. Lee, J. Kim, M. Paik, Y. Kim, K. Kim, M. Kim, T. Shin, and S. Il Seok, "Perovskite solar cells with atomically coherent interlayers on SnO_2 electrodes," Nature **598**, 444–450 (2021).
[55]Y.-H. Kim, S. Kim, A. Kakekhani, J. Park, J. Park, Y.-H. Lee, H. Xu, S. Nagane, R. Wexler, D.-H. Kim, S. Jo, L. Martínez-Sarti, P. Tan, A. Sadhanala, G.-S. Park, Y.-W. Kim, B. Hu, H. Bolink, S. Yoo, R. Friend, A. Rappe, and T.-W. Lee, "Comprehensive defect suppression in perovskite nanocrystals for high-efficiency light-emitting diodes," Nat. Photonics **15**, 148–155 (2021).
[56]Q. Zhang, M. Tavakoli, L. Gu, D. Zhang, L. Tang, Y. Gao, J. Guo, Y. Lin, S.-F. Leung, S. Poddar, Y. Fu, and Z. Fan, "Efficient metal halide perovskite light-emitting diodes with significantly improved light extraction on nanophotonic substrates," Nat. Commun. **10**, 727 (2019).